Bioactive Materials 33 (2024) 497–505

Contents lists available at ScienceDirect

Bioactive Materials

journal homepage: www.keaipublishing.com/en/journals/bioactive-materials

Biguanide chitosan microneedles with cell-free DNA scavenging ability for psoriasis therapy

Zihao Liu [1], Yu Wang [1], Yuhan Zhang [1], Liufu Hu [1], Bozhi Chen, Yang Li, Xindong Guo [**], Bingran Yu [***], Fu-Jian Xu [*]

State Key Laboratory of Chemical Resource Engineering, Key Lab of Biomedical Materials of Natural Macromolecules (Beijing University of Chemical Technology, Ministry of Education) and Laboratory of Biomedical Materials, Beijing University of Chemical Technology, Beijing 100029, China

ARTICLE INFO

Keywords:
Biguanide chitosan
cfDNA
Microneedles
Psoriasis

ABSTRACT

High levels of cell-free DNA (cfDNA) induce psoriasis. Currently, the treatment of psoriasis has the disadvantages of penetration difficulty, suppression of normal immunity, and skin irritation. In this study, biguanide chitosan microneedles (BGC-MNs) were prepared to treat psoriasis by removing cfDNA from the dermis through the skin barrier. The effects of chitosan with different bisguanidine contents on DNA-binding capacity, biocompatibility, and inflammation inhibition were compared, revealing that chitosan containing 20% bisguanidine (BGC2) was found to have the best overall performance. *In vitro,* BGC2 effectively cleared cfDNA and inhibited the production of inflammatory factors. BGC-MN made from BGC2 had good mechanical and solubility properties. *In vivo,* BGC-MNs cleared cfDNA, reduced the level of inflammatory factors in the dermis, and exerted a good therapeutic effect on mice with psoriasis. These results suggested that BGC-MNs provided a new approach to treating psoriasis in terms of scavenging cfDNA and exerting anti-inflammatory effects.

1. Introduction

Psoriasis is a common chronic inflammatory skin disease [1,2]. The main manifestation of psoriasis is a thickening of the epidermis and dermis [3,4]. Current clinical drugs for treating psoriasis are mainly based on vitamin D series and glucocorticoids, but long-term drug therapy irritates the skin and weakens immunity. In addition, vitamin D series and glucocorticoids treat only mild and moderate psoriasis [5]. For severe psoriasis, immunosuppressive therapy is the main approach, including the use of cyclosporine and tacrolimus [6,7]. However, the immunosuppressive agents inhibit the normal immune response and reduce the ability to fight pathogens [8,9]. An abnormal increase in the amount of cfDNA has been identified as a pathogenetic source in several inflammatory diseases, such as rheumatoid arthritis, acute liver failure, and systemic lupus erythematosus [10–13]. The current studies have shown that the elevated level of cfDNA abnormally activates immune cells, leading to the development of psoriasis [14–16]. Therefore, scavenging cfDNA is essential to inhibit inflammatory responses.

Some studies demonstrated that cationic polymers could scavenge cfDNA in the blood [17]. Patients with psoriasis had more cfDNA in the blood than healthy people [18]. Also, a clear distribution of cfDNA was observed in psoriatic lesions [19]. Besides scavenging cfDNA in the blood, it is necessary to scavenge cfDNA in the skin for treating psoriasis. At present, a treatment method with cationic polymers for psoriasis involves coating with cream [20]. However, the cream may cause skin irritation in some patients. The thickening of psoriatic skin also has an adverse effect on drug penetration. Recently, microneedles (MNs) have attracted much attention for transdermal drug delivery [21]. The micronized size penetrates the epidermis painlessly, creates reversible skin channels, and facilitates the smooth entry of drug molecules into the dermis [22]. MN treatment is a better method than coating for treating psoriasis. To the best of our knowledge, MNs made of DNA scavengers are rarely reported. The mechanical properties of DNA scavengers may not meet the requirements of microneedles to penetrate

Peer review under responsibility of KeAi Communications Co., Ltd.
* Corresponding author.
** Corresponding author.
*** Corresponding author.
E-mail addresses: xdguo@buct.edu.cn (X. Guo), yubr@mail.buct.edu.cn (B. Yu), xufj@mail.buct.edu.cn (F.-J. Xu).
[1] These authors contributed equally to this work.

https://doi.org/10.1016/j.bioactmat.2023.11.015
Received 1 August 2023; Received in revised form 20 November 2023; Accepted 21 November 2023

skin. Therefore, we designed cationic MNs to solve the penetration problem and scavenge cfDNA in the dermis.

Chitosan, as a biocompatible polysaccharide, has a variety of applications in drug delivery [23]. The high intermolecular force of chitosan provides a mechanical basis for the fabrication of MNs. Chitosan MNs have the potential to reach the dermis. However, the electrostatic interaction between chitosan and DNA is not strong [24,25]. If chitosan is modified into a cationic polymer with strong DNA-binding ability, it is expected to provide a new material for scavenging cfDNA in the dermis.

Based on the background, we designed cationic MNs based on chitosan for scavenging cfDNA in the dermis (Fig. 1). Chitosan was modified with biguanide. A series of biguanide chitosan (BGC) with different DNA-binding abilities were prepared by regulating biguanide content in chitosan. After three types of BGCs were compared *in vitro*, one type of BGC was obtained with excellent DNA-binding ability, biocompatibility, and anti-inflammatory effect. BGC-MNs were made from BGC, and then the ability to scavenge cfDNA safely was proved in a mouse model of psoriasis.

2. Results and discussion

2.1. Preparation of biguanide chitosan

Chitosan is a cationic polysaccharide rich in amino groups. Its water solubility is poor because of intramolecular hydrogen bonds. Biguanide is a strong positive functional group. The introduction of biguanide not only enhanced the positive charge but also disrupted the intramolecular hydrogen bond and then improved water solubility of BGCs. First, the water-soluble chitosan hydrochloride (CS•HCl) was obtained. Then, the chitosan containing biguanide was obtained by adding an amino group from chitosan hydrochloride and a cyano group. By controlling the concentration of dicyandiamide and the reaction time, a series of BGCs with different bis-guanidinium contents were obtained, and the nitrogen contents of different BGCs were obtained by elemental analysis as 6.83%, 7.02% and 24.68%, respectively, and the guanidinium contents of the BGCs were obtained by calculations, and the results are shown in Table 1. Chitosan with 2% biguanide was named BGC1, chitosan with 20% biguanide was named BGC2, and chitosan with 40% biguanide was named BGC3.

Table 1
Reaction conditions of biguanide chitosan (BGC).

	CS•HCl (g)	Water (mL)	Dicyandiamide (g)	Time (h)	Biguanide content (mol%)
BGC1	0.7	10	0.5	3	4
BGC2	0.7	10	2.1	3	20
BGC3	0.7	10	2.1	10	40

2.2. DNA-binding ability and biocompatibility

The positive charge of BGCs is different from that of chitosan. Therefore, the change in the biguanide content impacts DNA-binding ability. Firstly, the DNA-binding ability of BGCs in an aqueous solution was evaluated (Fig. 2A). During the agarose gel electrophoresis experiment, when the mass ratio of BGC1/DNA was less than 0.5, the brightness of the migrated DNA band was seen for BGC1 with low biguanide content, indicating that a large portion of the DNA was not complexed. When the mass ratio of BGC1/DNA exceeded 0.5, DNA was complexed. BGC2 with medium biguanide content and BGC3 with high biguanide content exhibited high DNA-binding efficiency when the mass ratios of BGC2/DNA and BGC3/DNA were both 0.25.

The DNA-binding ability in serum also needs to be evaluated due to the presence of serum in tissues (Fig. 2B). Under 10% fetal bovine serum (FBS) conditions, when the mass ratio of BGC1/DNA was 0.5, a part of DNA was released. The reason was that the negatively charged part from FBS competed with the DNA. BGC2 and BGC3 had more biguanide than BGC1. Therefore, FBS could not compete with BGC2 and BGC3. The mass ratio of binding DNA was not altered in 10% FBS.

The binding of BGCs to DNA was verified in the presence of heparin to avoid electronegative substances affecting the binding of BGCs to intracellular cfDNA (Fig. 2C). For BGC1, DNA was completely released at a mass ratio of 0.25 in a heparin solution. However, partial DNA bound at a mass ratio of 0.25 in an aqueous solution. DNA was fully complexed at a mass ratio of 0.5. For BGC2 and BGC3, partial

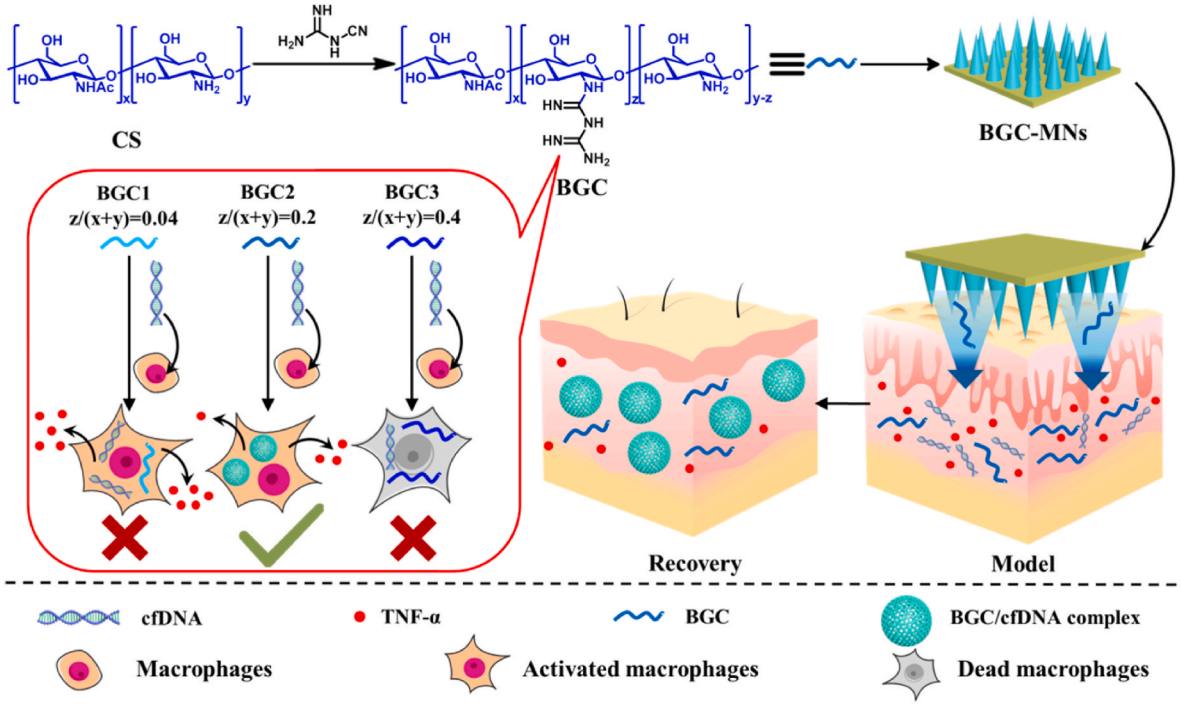

Fig. 1. Schematic illustration of topical therapy by scavenging cfDNA for psoriasis skin.

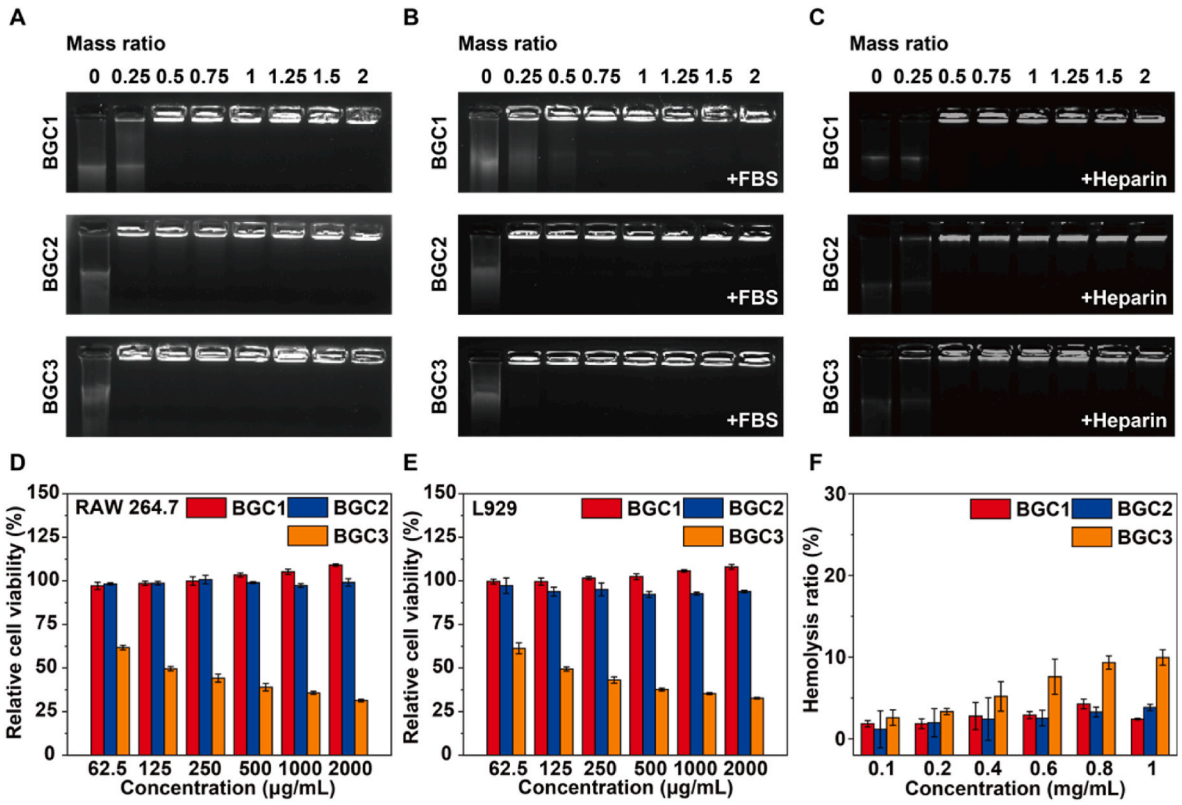

Fig. 2. (A)–(C) Electrophoretic mobility retardation assay of ctDNA in complexes with BGC1, BGC2 and BGC3 in water, FBS and heparin at various mass ratios. (D) and (E) Cytotoxicity of BGC1, BGC2 and BGC3 at various concentrations in RAW 264.7 cell lines and L929 cell lines. (F) Hemolysis ratio of RBCs treated with BGC1, BGC2 and BGC3 at various concentrations.

dissociation of BGC2/DNA and BGC3/DNA was observed at a mass ratio of 0.25. However, BGC2/DNA and BGC3/DNA still bound a large portion of the DNA at a mass ratio of 0.5. It indicated that heparin sodium competed for part of the DNA. However, BGC2 still bound DNA efficiently in the presence of heparin.

BGC1, BGC2, and BGC3 bind DNA at various mass ratios. However, a difference in DNA-binding ability was observed. BGC1 had the weakest DNA-binding ability and BGC2 and BGC3 had similar DNA-binding abilities because BGC1 had the least biguanide and the weakest electropositivity. Although BGC3 had more biguanide than BGC2, the DNA-binding ability of BGC2 was similar to that of BGC3 because both BGC2 and BGC3 had bound a large amount of DNA.

We first examined the cytotoxicity of BGCs in the mouse monocyte macrophage leukemia cell line (RAW 264.7) and mouse fibroblast cell line (L929) to verify its biocompatibility (Fig. 2D and E). Chitosan protected growth factors in the cell culture medium and then improved cell viability [26]. BGCs were obtained from chitosan and improved cell viability by protecting growth factors. In RAW 264.7 cells, BGC1 had a low positive charge, with few side effects on cells. The cell viability in the BGC1 group increased slowly with an increasing concentration from 62.5 μg/mL to 2000 μg/mL. The cell viability in the BGC2 group was almost unchanged at approximately 100%. Although BGC2 protects against growth factors, it has some effect on the cells due to the excessive positive charge. Under the combined effect of these two factors, the cell survival rate of BGC2 was almost 100%. On the other hand, the cell viability of the BGC3 group decreased because the strong positive charge affected the growth activity of the cells, which partially exceeded the protection of the growth factors. L929 cells were also used to evaluate the biocompatibility of BGCs due to epithelial cells in skin tissues. The experimental results of L929 cells were similar to those of RAW 264.7 cells. It indicated that the cell activity of BGCs was mainly affected by the positive charge. Combining the effects of BGCs on RAW 264.7 cells and L929 cells, the cytotoxicity of BGC1 and BGC2 was low, while the cytotoxicity of BGC3 was high.

RBCs (red blood cells) were exposed to BGCs during treatment, so the blood compatibility of BGCs was also an important indicator of biocompatibility. The hemolysis properties of three types of BGCs were tested to evaluate the blood compatibility of the three types of BGCs (Fig. 2F). Phosphate-buffered saline and 1% TritonX-100 were used as negative control and positive control, respectively. When the concentration of BGCs were 0.1, 0.2, 0.4, 0.6, 0.8, and 1 mg/mL, the hemolysis ratio of BGC1 was less than 5%. BGC2 also showed a hemolysis ratio similar to that of BGC1 indicating that BGC2 had good blood compatibility. However, when the BGC3 concentration was more than 0.4 mg/mL, the hemolysis ratio was higher than 5%. Therefore, the blood compatibility of BGC3 was poor. The biguanide content of BGC3 was higher than that of BGC2 and BGC1, which resulted in strong electrostatic interaction between BGC3 and erythrocytes. The electrostatic interaction led to the rupture of erythrocytes and the release of hemoglobin. Because BGC1 and BGC2 had low biguanide content, they did not cause the rupture of erythrocytes. Therefore, BGC1 and BGC2 had good blood compatibility, whereas BGC3 had poor blood compatibility.

2.3. *Effect of BGC on cfDNA-driven inflammation in vitro*

We labeled BGCs with fluorescein isothiocyanate (FITC). Then, we calculated the phagocytosis ratio by flow cytometry after RAW 264.7 cells were cultured with BGCs for 4 h to study the uptake of BGC by macrophages (Fig. 3A). The positive ratio was 53.4% for BGC1, 71.5% for BGC2, and 82.5% for BGC3. According to the findings, an increase in biguanide content led to an increase in electropositivity and phagocytosis ratio. cfDNA causes macrophage polarization after it is taken up by macrophages [10]. If cationic material is used to bind cfDNA in macrophages, the macrophages are polarized into anti-inflammatory

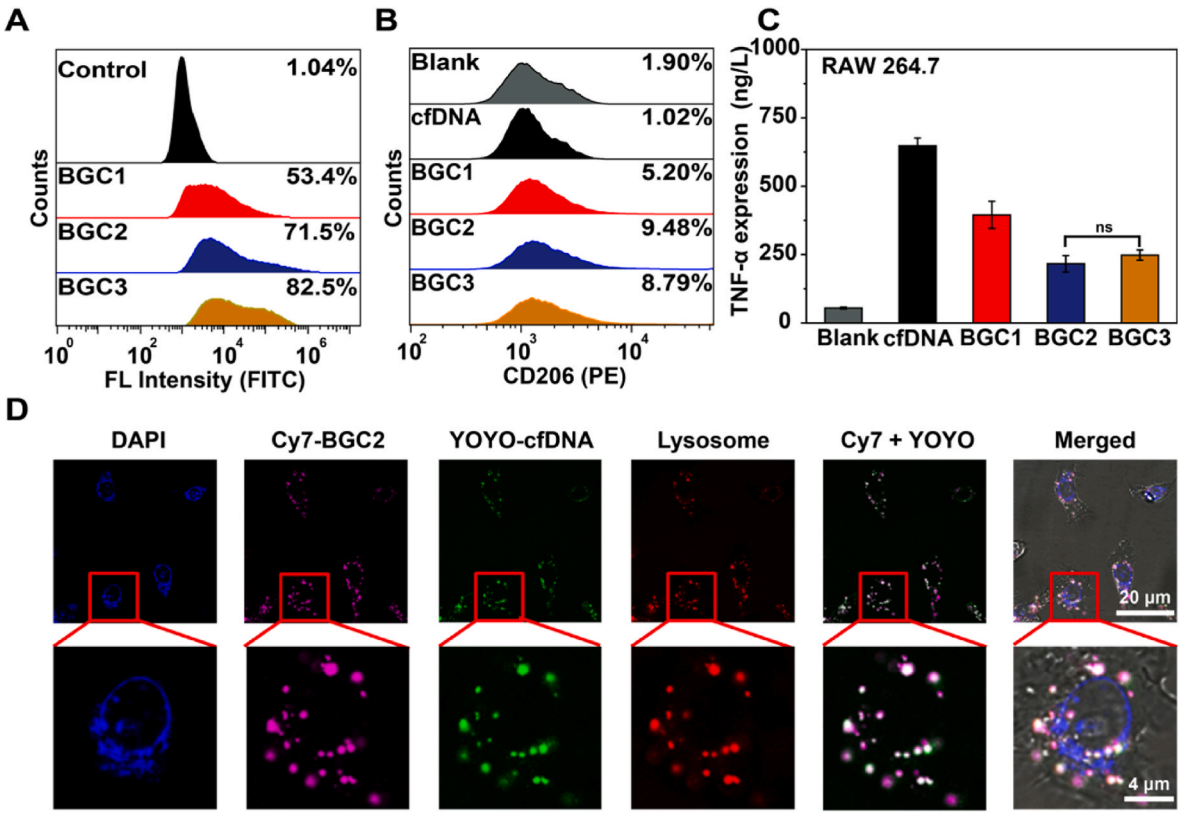

Fig. 3. (A) Flow cytometry results of RAW 264.7 cells treated with BGC1, BGC2 and BGC3 for 4 h. (B) CD206 on macrophages by flow cytometry. (C) BGC1, BGC2 and BGC3 inhibited TNF-α expression in RAW 264.7 cell (D) CLSM images and enlarged images show intracellular localization of intracellular cfDNA and BGC2 in RAW 264.7 cells after 4 h incubation. Colocalization of cfDNA and BGC2 showed up as white spots.

M2-type macrophages [27]. CD206 is the marker of M2-type macrophages [28]. The expression of CD206 in macrophages was detected by immunofluorescence staining to evaluate the anti-inflammatory effect of BGCs (Fig. 3B). The positive ratio of CD206 in the BGC1 group was 5.20%, indicating that BGC1 promoted the differentiation of M2-type macrophages. The positive ratio of CD206 in the BGC2 and BGC3 groups was 9.48% and 8.79%, respectively. The flow cytometry analysis showed that the positive ratio of CD206 in the cfDNA group was only 1.02%, which was similar to 1.90% in the Blank group. It indicated that BGC2 and BGC3 had similar abilities to polarize into M2-type macrophages; however, their ability was better than that of BGC1. The results were consistent with the results of DNA binding (Fig. 2A and B).

After cfDNA was taken up by macrophages, the macrophages secreted various types of inflammatory cytokines, such as tumor necrosis factor-α (TNF-α) and interleukin-6 (IL-6) [10]. The inflammatory factors caused tissue and organ damage [29]. Therefore, we evaluated the downregulation of TNF-α and IL-6 in RAW 264.7 cells using enzyme-linked immunosorbent assay (Fig. 3C and Suppl. Fig. S1). In the test for TNF-α, the expression of TNF-α was the lowest in the Blank group because RAW 264.7 cells were not stimulated by cfDNA and did not secrete TNF-α. In the cfDNA group, RAW 264.7 cells secreted a large amount of TNF-α after being stimulated by cfDNA. In the BGC1 group, BGC1 was added to RAW 264.7 cells after being stimulated by cfDNA and then a part of cfDNA was complexed. Therefore, the stimulation process was partially blocked. It resulted in a decrease in the expression of TNF-α. In the BGC2 and BGC3 groups, cfDNA stimulated RAW 264.7 cells, but RAW 264.7 cells also took up BGC2 and BGC3. BGC2 and BGC3 bound most of cfDNA, which severely inhibited the cfDNA-mediated secretion of inflammatory factors. Therefore, the expression level of TNF-α was higher in the BGC2 and BGC3 groups than in the Blank group but lower than in the BGC1 group. The expression of TNF-α in the BGC2 and BGC3 groups was similar because both BGC2 and BGC3 could bind most of cfDNA. The IL-6 test showed a similar trend to the TNF-α test. These results indicated that BGCs inhibited the secretion of inflammatory cytokines. The anti-inflammatory effects of BGC2 and BGC3 were better than that of BGC1. Combining DNA-binding ability, biocompatibility, and anti-inflammatory effects, BGC2 (25 μg/mL) was the best material for biological applications and was selected for subsequent experiments. To further observe the toxicity of BGC2, we also performed cytotoxicity experiments with different concentrations of BGC2 in Human immortal keratinocyte line (HaCaT) as well as in serum-free conditions in L929 (Suppl. Figs. S7 and S8), The results confirmed the low cytotoxicity of BGC2 in L929 even in the absence of serum interference and virtually no toxicity in the HaCaT cell line, suggesting that BGC2 is safe enough to be used to carry out subsequent cell and animal experiments. The production of inflammatory cytokines by cfDNA is realized in the lysosome [17]. Therefore, it is essential to demonstrate the entry of BGC2 into lysosomes. The intracellular validation was designed using YOYO-labeled cfDNA and cyanine 7 (Cy7) -labeled BGC2 (Fig. 3D). At a low magnification of confocal laser scanning microscope (CLSM) images, RAW 264.7 cells universally took up cfDNA and BGC2. RAW 264.7 cells still took up BGC2 after cfDNA entered into RAW 264.7 cells. The phagocytosis ratio of BGC2 detected by the CLSM experiment was similar to that observed by flow cytometry. At a high magnification of CLSM images, both cfDNA and BGC2 were found to be located in lysosomes. It indicated that BGC2 bound to cfDNA in lysosomes and then inhibited the process in which cfDNA stimulated macrophages to produce inflammatory factors.

2.4. Characterization of BGC2-MNs

To treat psoriasis in a minimally invasive manner, we prepared BGC2-MNs by vacuum-filling BGC2 solution into the cavity of polydimethylsiloxane (PDMS) negative mold and delivering it into the skin.

The dried BGC2-MNs had a complete needle body and a sharp needle tip (Fig. 4A). The SEM images demonstrated that the surface of BGC2-MNs was smooth, indicating that the BGC2 was completely into the PDMS negative mold (Fig. 4B). BGC2-MNs was not defective in preparation. The resulting BGC2-MNs comprised a 5 × 5 array, and each needle consisted of a 350-μm base diameter and 650 μm height. The height of BGC2-MNs was beneficial to the penetration of the stratum corneum (SC) and the opening of the skin channel [30]. The fracture strength of BGC2-MNs was analyzed by applying an axial compressive load to BGC2-MNs with a certain force generated by the force test. The force–displacement curve of the compressive force of BGC2-MNs showed that the axial force was positively correlated with the displacement (Fig. 4C). The needle tip bent without fracture at 0.2 N. When the force was greater than 0.2 N, the needle began to fail. The minimum-required force to penetrate the stratum corneum (SC) was 0.058 N [31]. The height and mechanical properties of BGC2-MNs were consistent with those described in the literature. BGC2-MNs had sufficient properties to penetrate the skin. Rhodamine B-loaded BGC2-MNs (RhoB-loaded BGC2-MNs) were used to observe the penetration performance of BGC2-MNs. Each needle of the 5 × 5 BGC2-MNs penetrated the skin (Fig. 4D). It indicated that the insertion effect of BGC2-MNs was outstanding.

By observing the dissolution of microneedles in gelatin and pig skin at different time points (Suppl. Fig. S2), it was seen that the height of microneedles decreased with the increase in the stabbing time. The height decreased faster in 5 min after the stabbing, indicating that the tip part of the microneedles dissolved faster and the decreasing tendency slowed down after 5 min, showing that the needle part of the microneedles dissolved more slowly and the microneedles were completely dissolved in 20 min after stabbing. The dissolution performance of the material was good.

To ensure that BGC2-MNs were used in the skin of patients with psoriasis, we observed the penetration of BGC2-MNs into the parafilm that mimicked psoriatic skin (Suppl. Fig. S3) [32]. It was seen that the insertion ratio of needles was 100% in the first layer and 96% in the second layer. The thickness of the SC was generally less than 200 μm [33]. The thickness of the two layers of the parafilm was about 250 μm. This indicated that BGC2-MNs passed through the mechanical protection of psoriatic skin. The thickness of the epidermis in patients with psoriasis was generally less than 600 μm [33]. The height of BGC2-MNs was 650 μm, and BGC2-MNs could deliver BGC2 into the psoriatic skin. The mechanical property and height of BGC2-MNs were sufficient for treating patients with psoriasis.

Optical coherence tomography was used to observe the dissolution of BGC2-MNs in mouse skin (Fig. 4E and Suppl. Fig. S4). It was observed that the BGC2-MNs were successfully pierced subcutaneously. BGC2-MNs were gradually dissolved subcutaneously in the skin at 5 min to 30 min. At 5 min–10 min, the degree of dissolution of the body of the needle did not change significantly, probably due to the short time interval, but by 20 min, the body of the needle had dissolved most of the

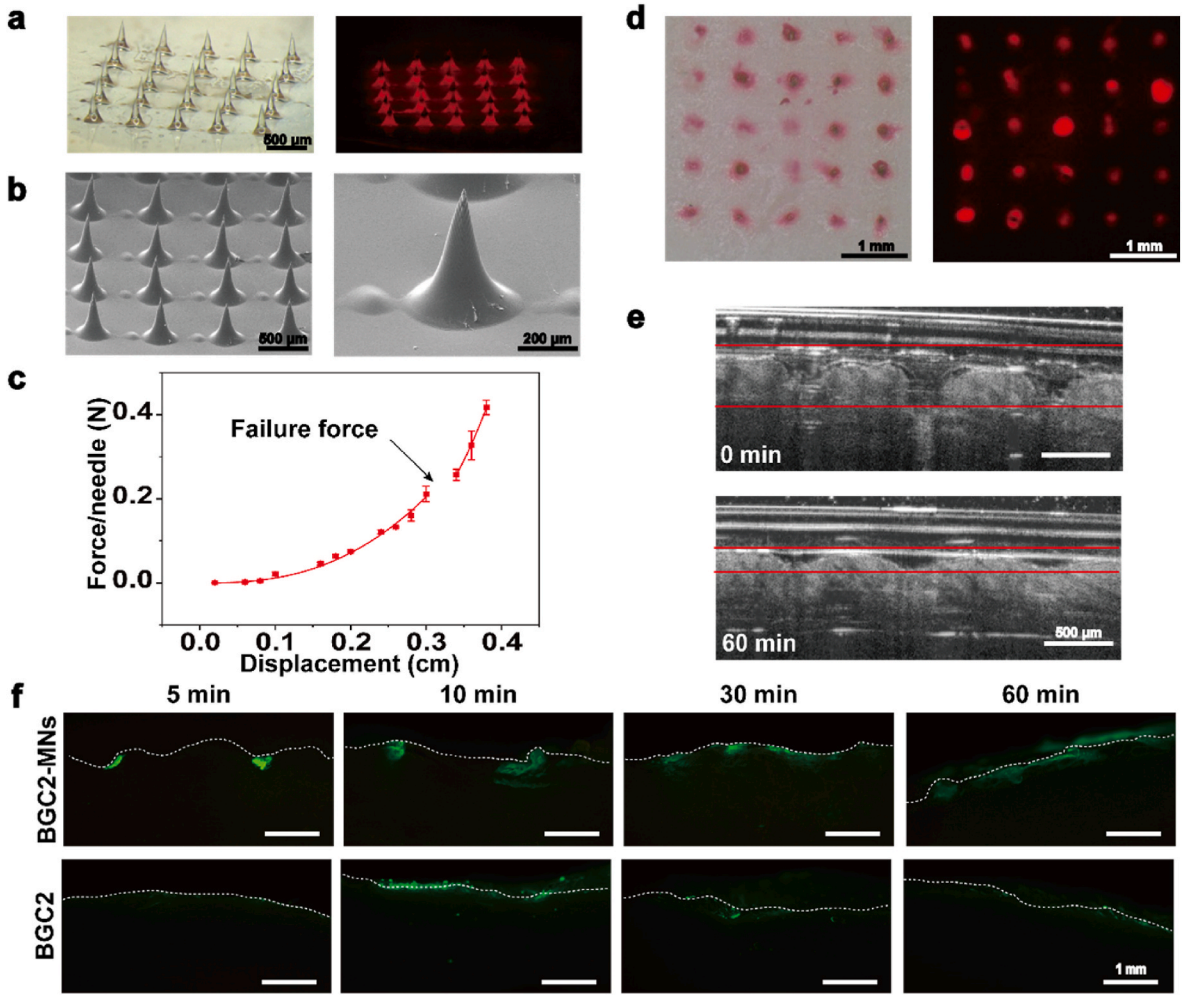

Fig. 4. (A) Bright-field image and fluorescence images of BGC2-MNs and RhoB-loaded BGC2-MNs. (B) SEM images of BGC2-MNs. (C) Mechanical behavior of BGC2-MNs. (D) Photographs of RhoB-loaded BGC2-MNs punctured the porcine skin. (E) Recovery of mice skin after insertion of BGC2-MNs observed by optical coherence tomography. (F) Fluorescence microscopy images of porcine skin being penetrated by FITC-labeled BGC2-MNs and FITC-labeled BGC2 at different time points.

way, and at 30 min the body of the needle had basically dissolved. After 60 min, the pinholes are almost healed, but due to the elasticity of the skin, the compressed area has not yet completely returned to a smooth state. Then, we observed the subcutaneous penetration of FITC-labeled BGC2-MNs (microneedles) and FITC-labeled BGC2 (coating) at different time points under a fluorescence microscope to evaluate the penetration of BGC2 in the skin (Fig. 4F). In 10 min, obvious fluorescence accumulation inside the skin was noted in the BGC2-MNs group, whereas the fluorescence in the BGC2 group was distributed on the surface. In 30 and 60 min, fluorescence penetration in the skin gradually increased in depth and area in the BGC2-MNs group. The diffusion depth was lower in the BGC2 group than in the BGC2-MNs group. This is because SC assumes the main barrier role of the skin and is highly lipophilic, and our synthesized BGC2 is a hydrophilic polymer and is therefore not suitable for penetrating SC. This problem was facilitated by making BGC2 into microneedles to facilitate the penetration of BGC2, which allowed BGC2 to work deeper into the lesion site.

2.5. Skin symptoms of psoriasis after treatment

BGC2-MNs were used to treat imiquimod (IMQ)-induced psoriasis-like mouse model to evaluate the therapeutic effect in vivo. This model was used as an acute psoriasis-like mouse model because it partly triggered dermatitis similar to human psoriasis. After applying IMQ to the back for 5 days, the skin inflammation was successfully induced with the symptoms of erythema and scaling, indicating the onset of psoriasis. *In vivo,* IMQ-induced mice showed higher psoriasis area and severity index (PASI) scores than normal mice. Topical application of BGC2 to psoriatic skin on the back using coatings (BGC2 group), microneedles (BGC2-MNs group), or clinical medication Capotriol ointment (Cal) for 4 days (Fig. 5A and B and Suppl. Fig. S5). Under the action of BGC2-MNs, BGC2 easily entered the epidermis and dermis and improved its therapeutic effect. Compared to the clinical drug Cal, the BGC2-MNs group was able to treat psoriasis more rapidly and effectively in terms of therapeutic efficacy. The PASI scores in the BGC2-MNs group were similar to those in the Normal group. This proved that BGC2-MNs were beneficial to skin penetration, and BGC2 could treat psoriasis. However, the coating (BGC2 group) only entered the skin through the hair follicle. Therefore, BGC2 utilization efficiency was low. During the treatment period, erythema disappeared, but some scales persisted, and the degree of skin hypertrophy remained unchanged in the Model group because mice partially regulated autoimmune diseases. The Cal group was able

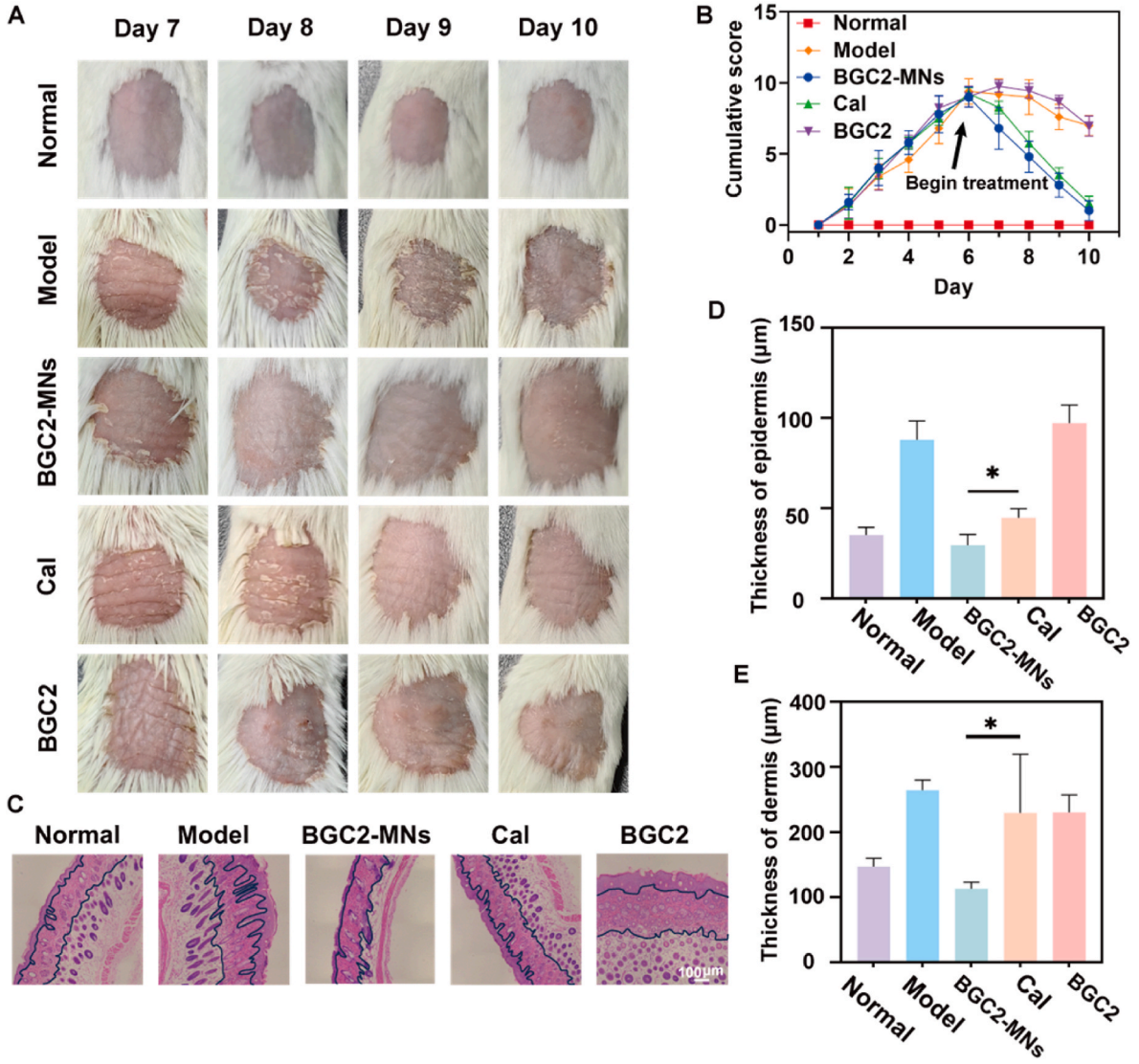

Fig. 5. (A) Representative skin surface morphology of the various groups during treatment. (n = 5). (B) The cumulative score of erythema, scale, and thickness scores of mouse back skin. (C) H&E staining of back skin after treatment. (The black dotted line in the diagram is to distinguish between the epidermis, dermis and subcutaneous tissue of the skin) (D) and (E) Analysis of the thickness of the epidermis and dermis of mouse back skin in H&E stained sections.

to treat psoriasis better compared to the BGC2 group, but not as well as the BGC2-MNs group in terms of speed of treatment and final outcome. The PASI scores in the BGC2 group were similar to those in the Model group. The effects on physiological activities were then evaluated by the changes in body weight (Suppl. Fig. S6). No significant change was found in the body weight of mice in each group during modeling and treatment, which proved the safety of BGC2.

When mice developed psoriasis, the skin showed definite histopathological changes (Fig. 5C–E). In IMQ-induced mice, the epidermis and dermis were significantly thickened. In addition, the epidermal rete ridges became markedly elongated and even formed long and thin undulations that extended down into the dermis. A better therapeutic effect was observed in the BGC2-MNs group than in the BGC2 and Cal group, including a significant reduction in epidermal and dermal thickness and normal epidermal reticulum ridge. The pathological features in the BGC2-MNs group were similar to those in the Normal group. It indicated that BGC2-MNs improved the skin pathological symptoms of psoriasis. In the BGC2 group, these pathological symptoms were alleviated in IMQ-induced mice, but the epidermal and dermal thickness was higher than that in the Normal group.

2.6. Characterization of inflammation after treatment of psoriasis

The spleen is the largest immune organ. Once the immune system is stimulated, the spleen produces the corresponding immune response. The inflammation causes swelling of the spleen [34]. We analyzed the inhibitory effect of BGC2-MNs on inflammation from pathological sections and the weight fraction of the spleen to the body (Fig. 6A and B). The spleen cells in the BGC2-MNs group were dense and well arranged, similar to those of healthy mice, indicating that the spleen did not develop lesions. The spleen cells in the BGC2 group and the model group were disorganized and had many gaps, suggesting abnormal changes in the spleen, while the morphology of the spleen cells in the BGC2-MNs group was also better than that of the Cal group. According to the spleen weight fraction of the body, the spleen weight fraction of the body in the model group and the BGC2 group reached much higher than that of healthy mice, which indicated that splenomegaly occurred. The spleen weight fraction of the BGC2-MNs group was lower than that of the other treatment groups and was similar to that of the healthy mice, which corresponded to the data of the HE, suggesting that the BGC2-MNs had a very good inhibitory effect on the splenic lesions. In addition since splenomegaly is almost caused by inflammatory reactions in vivo. Combined with the analysis of splenic lesions, it may indicate that BGC2-MNs have a strong role in suppressing inflammation conveniently. We therefore examined the inhibitory effect of BGC2-MNs on inflammation by immunohistochemical staining (IHC) of tissues and detection of inflammatory factors in serum. (Fig. 6C and D). A number of inflammatory factors such as IL-17 (interleukin-17) and IL-23 (interleukin-23) TNF-α play an important role in the production and development of psoriasis. By immunohistochemical staining of the lesion tissues, the results showed higher levels of inflammatory factors in the skin of the model group and a slight downregulation of BGC2, but the reduction of inflammatory levels in the BGC2-MNs compared to the BGC2 and Cal groups was more pronounced and even similar to that of the healthy mice. This suggests that although BGC2 can enter the skin through the hair follicle, the effect is not satisfactory, and BGC2-MNs can promote the entry of BGC2 into the skin, which can better inhibit the development of inflammation. In a mouse model of psoriasis, the affected area not only oversecreted inflammatory cytokines but also altered multiple immune cell types associated with skin homeostasis [35]. An increase in the number of macrophages and T cells at the psoriasis site led to an overproduction of inflammatory cytokines [2]. The IHC of immune cells showed changes in the number of macrophages ($CD68^+$) and T cells ($CD3^+$) in psoriasis [19]. Treatment with BGC2-MNs reduced the infiltration of immune cells compared to the model, BGC2 and Cal groups, indicating that BGC2-MNs had a good inhibitory effect on inflammation. In order to understand the inflammation level situation in the body, several inflammatory factors (TNF-α, IL-1β, IL-6, IL-17, IL-23) in serum were also measured. The results showed that BGC2-MNs had the best anti-inflammatory effect and reduced the level of inflammation in the body compared to other groups. Combined with the immunohistochemical results and serum levels of inflammatory factors, both indicate that BGC2-MNs is an excellent drug for the treatment of psoriasis.

2.7. Organ hematoxylin and eosin staining and biochemical factor analysis

The tissue damages caused by BGC2-MNs in the heart, liver, lung, and kidney were determined using hematoxylin-eosin (H&E) staining (Fig. 7A). No significant damage and inflammation were found in the major organs of each group, which confirmed that BGC2-MNs had little systemic toxicity. The hepatotoxicity of BGC2-MNs was reflected by alanine transaminase (ALT), alkaline phosphatase (ALP) and aspartate transaminase levels and nephrotoxicity was reflected by creatinine (CREA), uric acid, and urea (Fig. 7B). It showed that the levels of biochemical factors were similar in each group. It indicated that BGC2 did not affect the liver and kidneys. The organ H&E and biochemical factor analysis indicated that BGC2-MNs had excellent biocompatibility.

2.8. In vivo imaging on skin

We observed the metabolism of FITC-labeled BGC2-MNs in mouse skin, and as can be seen from Suppl. Fig. S9A,B, the fluorescence intensity gradually decreased with time, indicating that BGC2-MNs were metabolised in vivo after entering the skin. As the fluorescence intensity of BGC2-MNs decreased dramatically at 24 h. In order to observe the main metabolic organs of BGC2-MNs, its heart, liver, spleen, lungs and kidneys were obtained by dissection to observe the fluorescence intensity at 24 h when the microneedle was lodged into the skin, as shown in Suppl. Fig. S9C, which shows that the BGC2 was mainly metabolised from the liver and kidneys.

3. Conclusions

In this study, we synthesized three types of BGCs and evaluated their properties for potential application in microneedles. Among them, BGC2 exhibited outstanding DNA binding ability, high biosafety, and excellent anti-inflammatory effects. Considering the challenges posed by the skin barrier in delivering drugs for the treatment of skin diseases like psoriasis, our BGC2 preparation method, which is simple and high-yielding, holds great promise. To address the issue of drug permeability, we successfully fabricated BGC2 microneedles (BGC2-MNs) with excellent mechanical properties using a single component of BGC2. These BGC2-MNs effectively improved the efficacy of inhibiting inflammation by efficiently delivering and binding DNA. Our findings highlight the potential of BGC2-MNs as a promising therapeutic approach for skin diseases. These results contribute to the development of high-quality microneedle-based drug delivery systems for large-scale production.

CRediT authorship contribution statement

Zihao Liu: Writing – original draft, Methodology. **Yu Wang:** Writing – original draft, Methodology, Formal analysis. **Yuhan Zhang:** Formal analysis. **Liufu Hu:** Methodology. **Bozhi Chen:** Data curation. **Yang Li:** Data curation. **Xindong Guo:** Conceptualization. **Bingran Yu:** Writing – review & editing, Funding acquisition, Conceptualization. **Fu-Jian Xu:** Funding acquisition, Conceptualization.

Declaration of competing interest

The authors declare that they have no known competing financial

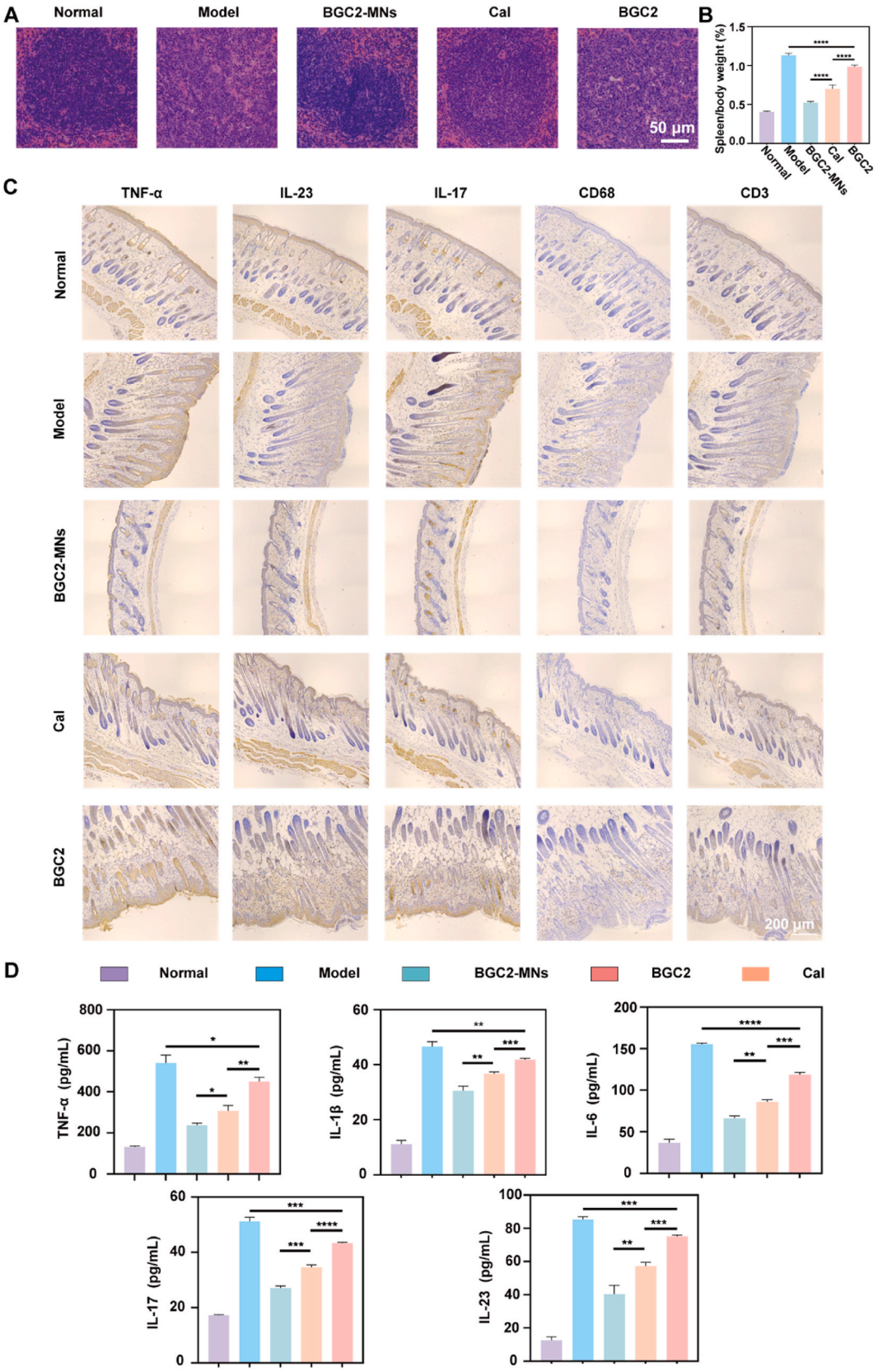

Fig. 6. (A) H&E staining images of spleen from various groups on the 10th day. (B) Spleen weight normalized to body weight on the 10th day. (C) Immunohistochemical staining of mouse back skin. (D) The measurement of cytokines of TNF-α, IL-1β, IL-6, IL-17 and IL-23 in the serum after different treatments by ELISA kits. Data were expressed as the mean ± SD ($n = 3$).

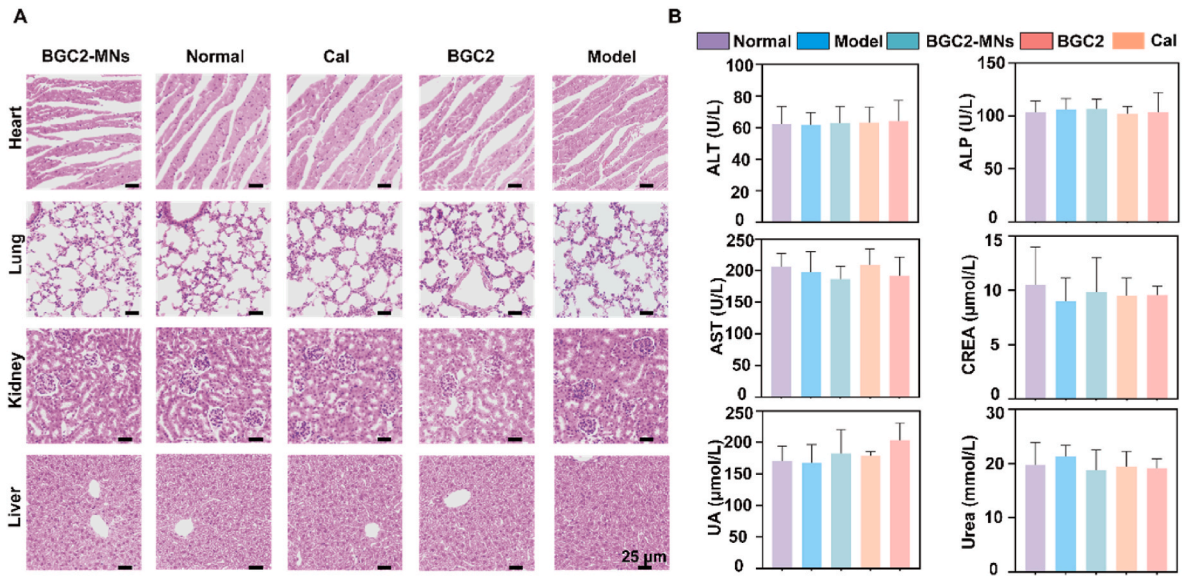

Fig. 7. (A) H&E staining images of heart, liver, lung, and kidney from various groups. (B) ALT, ALP, AST, CREA, UA and urea analysis from various groups.

interests or personal relationships that could have appeared to influence the work reported in this paper.

Acknowledgements

Z.L., Y.W. and L.H. contributed equally to the study. This work was supported by National Key R&D Program of China (Grant number 2021YFB3800900), National Natural Science Foundation of China (Grant numbers 52073013, 22122501, 52221006 and 52161145410) and Beijing Outstanding Young Scientist Program (No. BJJWZYJH01201910010024). Animal studies were approved by the Ethical Committee of Chinese Academy of Medical Sciences (CAMS).

Appendix A. Supplementary data

Supplementary data to this article can be found online at https://doi.org/10.1016/j.bioactmat.2023.11.015.

References

[1] M. Lowes, A. Bowcock, J. Krueger, Nature 445 (2007) 866.
[2] F. Nestle, D. Kaplan, J. Barker, N. Engl. J. Med. 361 (2009) 496.
[3] C. Griffiths, J. Barker, Lancet 370 (2007) 263.
[4] W. Boehncke, M. Schoen, Lancet 386 (2015) 983.
[5] J. Miller, R. Gallo, Dermatol. Ther. 23 (2010) 13.
[6] J. Xia, S. Xie, K. Liu, L. Xu, P. Zhao, S. Gai, P. Guan, J. Zhao, Y. Zhu, L. Tsoi, P. Stuart, R. Nair, H. Yang, Y. Liao, K. Mao, M. Qiu, Z. Ying, B. Hu, Z. Yang, W. Bai, X. Zhu, P. Cong, J. Elder, Z. Ye, B. Wang, H. Zheng, Ann. Rheum. Dis. 79 (2020) 1460.
[7] A. Pacifico, M. Ardigò, P. Frascione, G. Damiani, A. Morrone, Br. J. Dermatol. 183 (2020) 375.
[8] P. Laetitia, D. Rosemary, W. Alain, P. Laura, Z. Mahmoud, S. Emilie, JAMA Dermatol. 157 (2021) 1056.
[9] X. Li, K. Andersen, H. Chang, J. Curtis, G. Alexander, Comparative risk of serious infections among real-world users of biologics for psoriasis or psoriatic arthritis, Ann. Rheum. Dis. 79 (2019) 285.
[10] H. Liang, B. Peng, C. Dong, L. Liu, J. Mao, S. Wei, X. Wang, H. Xu, J. Shen, H. Mao, Nat. Commun. 9 (2018) 4291.
[11] J. Wu, H. Liang, Y. Li, Y. Shi, M. Bottini, Y. Chen, L. Liu, Adv. Funct. Mater. 30 (2020), 2000391.
[12] J. Lee, J. Sohn, Y. Zhang, K. Leong, D. Pisetsky, B. Sullenger, Proc. Natl. Acad. Sci. U.S.A. 108 (2011), 14055.
[13] E. Holl, K. Shumansky, L. Borst, A. Burnette, C. Sample, E. Ramsburg, B. Sullenger, Proc. Natl. Acad. Sci. U.S.A. 113 (2016) 9728.
[14] M. Beranek, Z. Fiala, J. Kremlacek, C. Andrys, J. Krejsek, K. Hamakova, M. Chmelarova, V. Palicka, L. Borska, Arch. Dermatol. Res. 309 (2017) 815.
[15] R. Lande, J. Gregorio, V. Facchinetti, B. Chatterjee, Y. Wang, B. Homey, W. Cao, Y. Wang, B. Su, F. Nestle, Nature 449 (2007) 564.
[16] J. Kim, B. Kim, M. Jeong, S. Seo, M. Kim, C. Hong, B. Ro, J. Kor. Med. Sci. 20 (2005) 649.
[17] W. Da, M. Sun, Y. Zhao, D. Shao, H. Yan, Y. Lao, H. Hu, L. Cui, X. Lv, F. Liu, C. Chi, Y. Zhang, M. Li, M. Zhang, H. Tian, X. Chen, K. Leong, L. Chen, Sci. Adv. 6 (2020), eaay7148.
[18] S. Coimbra, C. Catarino, E. Costa, H. Oliveira, A. Figueiredo, P. Rocha, A. Santos, Br. J. Dermatol. 170 (2014) 939.
[19] H. Liang, Y. Yan, J. Wu, X. Ge, L. Wei, L. Liu, Y. Chen, Sci. Adv. 6 (2020), eabb5274.
[20] Y. Yan, H. Liang, X. Liu, L. Liu, Y. Chen, Biomaterials 276 (2021), 121027.
[21] D. Wu, X. Shou, Y. Yu, X. Wang, G. Chen, Y. Zhao, L. Sun, Adv. Funct. Mater. 32 (2022), 220584.
[22] C. Wang, Y. Ye, G. Hochu, H. Sadeghifar, Z. Gu, Nano Lett. 16 (2016) 2334.
[23] Z. Garaiova, S. Strand, N. Reitan, S. Lelu, S. Storset, K. Berg, Int. J. Biol. Macromol. 51 (2012) 1043.
[24] S. Rahmani, S. Hakimi, A. Esmaeily, E. Samadi, E. Mortazavian, M. Nazari, Z. Mohammadi, N. Tehrani, M. Tehrani, Int. J. Pharm. 560 (2019) 306.
[25] B. Deka, P. Bhattacharyya, Comput. Theor. Chem. 1051 (2015) 35.
[26] G. Howling, P. Dettmar, P. Goddard, F. Hampson, M. Dornish, E. Wood, Biomaterials 22 (2001) 2959.
[27] W. Geng, M. Chen, B. Tao, R. Wang, D. Wang, K. Li, C. Lin, X. Liu, P. Gao, Z. Luo, K. Cai, Appl. Mater. Today 26 (2022), 101351.
[28] Z. Gao, C. Zhang, N. Xia, H. Tian, D. Li, J. Lin, X. Mei, C. Wu, Acta Biomater. 126 (2021) 211.
[29] M. Feldmann, Annu. Rev. Immunol. 27 (2009) 1.
[30] D. Bi, F. Qu, W. Xiao, J. Wu, P. Liu, H. Du, Y. Xie, H. Liu, L. Zhang, J. Tao, Y. Liu, J. Zhu, ACS Nano 17 (2023) 4346.
[31] W. Chen, R. Tian, C. Xu, B. Yung, G. Wang, Y. Liu, Q. Ni, F. Zhang, Z. Zhou, J. Wang, G. Niu, Y. Ma, L. Fu, X. Chen, Nat. Commun. 8 (2017) 1777.
[32] C. Huang, K. Gou, X. Yue, S. Zha, R. Zeng, Y. Qu, C. Zhang, Mater. Des. 224 (2022), 111363.
[33] M. Alper, A. Kavak, A. Parlak, R. Demirci, I. Belenli, N. Yesildal, Braz. J. Med. Biol. Res. 36 (2003) 111.
[34] L. Liang, W. Fei, Z. Zhao, Y. Hao, C. Zhang, Y. Cui, X. Guo, Eur. J. Pharm. Biopharm. 164 (2021) 20.
[35] B. Flutter, F. Nestle, Eur. J. Immunol. 43 (2013) 3138.